


ENHANCING NOSE-TO-BRAIN DELIVERY OF PIRIBEDIL: DEVELOPMENT OF A NANOSUSPENSION DISPERSED IN NASAL IN-SITU GELLING SYSTEM

CHEKKILLA BHARGAVI^{1,2}, PATHURI RAGHUVeer^{1*} 

¹Department of Pharmaceutics, GITAM School of Pharmacy (Deemed to be University), Hyderabad, Telangana, India. ²Department of Pharmaceutics, Sarojini Naidu Vanita Pharmacy Maha Vidyalaya, Hyderabad, Telangana-502329, India
*Corresponding author: Pathuri Raghuv eer; Email: rpathuri@gitam.edu

Received: 27 Dec 2023, Revised and Accepted: 14 Feb 2024

ABSTRACT

Objective: This study focuses on improving the delivery of Piribedil, a poorly soluble drug, to the brain through the nasal route using a nanosuspension in a nasal in-situ gel.

Methods: The nanosuspension was prepared using the sonoprecipitation method. Quality-by-Design (QbD) principles were used to optimize both the formulation and process parameters. The optimal process parameters were determined as sonication time (7.09 min), sonication amplitude (83.44%), and infusion rate (2.41 ml/min) with a desirability value of 0.970.

Results: The nanosuspension exhibited an average particle size ranging from 46.7 nm to 50.1 nm, and polydispersity index values between 0.393 and 0.425. Zeta potential values ranged from -33.78±1.86 mV to -35.06±2.12 mV, indicating favorable stability. FTIR studies revealed molecular interactions between Piribedil and stabilizers. XRPD and DSC analyses showed the transition from a crystalline to an amorphous state in the nanosuspension. Dissolution studies demonstrated significantly accelerated dissolution for the Piribedil nanosuspension, attributed to its nanosize and improved wettability. Stability assessments confirmed the robustness of the nanosuspension.

Conclusion: This innovative approach offers potential solutions for drug solubility challenges and blood-brain barrier penetration, holding promise for effective brain-targeted treatments.

Keywords: Design of experiments, Process variables, Formulation variables, Intranasal delivery, Nanocrystals

© 2024 The Authors. Published by Innovare Academic Sciences Pvt Ltd. This is an open access article under the CC BY license (<https://creativecommons.org/licenses/by/4.0/>)
DOI: <https://dx.doi.org/10.22159/ijap.2024v16i3.50242> Journal homepage: <https://innovareacademics.in/journals/index.php/ijap>

INTRODUCTION

Dealing with disorders affecting the central nervous system (CNS) poses significant challenges due to the intricate nature of the blood-brain barrier (BBB). The BBB's complex structure creates formidable barriers that hinder the effective delivery of drugs to the CNS. This impediment significantly limits the success of therapeutic interventions for CNS-related conditions. Poor penetration of the BBB remains a substantial obstacle to the approval of over 90% of drugs targeting the CNS [1, 2]. Various methods have been explored to improve brain drug delivery, including invasive procedures like injecting drugs directly into the brain's ventricles or using implanted devices, each with its effectiveness and risks [3, 4]. Hence, there is a requirement for innovative drug delivery strategies capable of crossing the BBB without causing harm to brain cells, and this is where nanomedicine comes into play. Intranasal administration holds promise for CNS drug delivery [5, 6].

Nanosuspensions are a well-established method for producing nanoparticles, with their impact on improving the dissolution of drugs with poor water solubility has been extensively investigated in research [7]. Achieving effective intranasal drug delivery requires maintaining the drug within the nasal cavity for sufficient absorption while preventing dripping or reaching the throat [8]. To meet this requirement, nanoparticles have been integrated into mucoadhesive formulations, effectively combining the benefits of their nanoscale size with the ability to precisely target and adhere within the nasal cavity [9]. Numerous studies have documented the successful intranasal administration of nanosuspensions. For instance, Saindane *et al.* developed an in-situ gel containing a carvedilol-containing nanosuspension, while Hao *et al.* created a nanosuspension of resveratrol for brain delivery [10, 11]. Furthermore, meloxicam nanosuspensions have been introduced both in powder form and as sprays based on hyaluronate for systemic delivery [12, 13].

Piribedil functions as a dopamine agonist, effectively stimulating dopamine receptors in both the brain and peripheral dopaminergic pathways [14]. It's utilized to treat parkinson's disease and is available

as a 50 mg prolonged-release tablet [15]. However, its oral bioavailability remains under 10% with a brief elimination half-life of 2 h. As a result, the drug is currently prescribed 2-5 times daily, up to the highest permissible dosage is 250 mg per day [16]. Research spanning two decades has highlighted its ability not only to enhance motor symptoms but also to improve non-motor symptoms such as apathy and cognitive impairment. This improved attention to Piribedil suggests its potential for increased clinical application in the future [17-19]. Numerous approaches have been investigated to enhance the solubility of Piribedil, including the utilization of micelles [20], the development of solid lipid micro and nanoparticles [21], and the creation of hybrid nanoparticles using lecithin and chitosan [22].

Over the past decade, nanosuspensions of drug nanocrystals have evolved as a favorable method to enhance the solubility of hydrophobic drugs [23]. Their main benefit lies in augmenting bioavailability through the reduction of particle size and the amplification of the specific surface area of the particles. Furthermore, these formulations offer additional benefits, including consistent performance in fasted/fed states and easy administration [24-26].

The characteristics of drug particles in the nanosuspension can be tailored to adapt to changes in the digestive environment, including pH, polymer compositions, surface-active agents, ionic strength, enzymatic activities, and gastrointestinal motility during absorption [27]. Additionally, they can be surface-modified to selectively adsorb blood proteins, targeting specific sites like the brain or bone marrow [28]. To maintain stability, nanosuspensions require a third component known as a stabilizer, such as a surfactant and/or polymer. Electrostatic and steric stabilizers play a crucial role in preventing particle aggregation. Combining these mechanisms is often referred to as "electrosteric stabilization," achieved through stabilizers containing both polymeric chains and charged groups or by combining non-ionic polymers and anionic surfactants [29]. This choice of stabilizers and their concentrations significantly influences particle size and the kinetics of size reduction [30]. The pursuit of achieving a stable particle size with diverse stabilizers and process parameters can be a complex endeavor [31-33].

The quality of pharmaceutical formulations depends on critical variables such as the active pharmaceutical ingredient (API), excipients, their concentrations, and the manufacturing process. QbD approaches involve predicting and achieving formulation quality by controlling relevant parameters and reducing the wastage of excipients inherent in trial-and-error approaches. Successful QbD application necessitates the comprehensive study of formulation variables and their interactions [34, 35].

Applying QbD to nanosuspension formation involves statistical experimental designs to analyze formulation parameter interactions. Statistical design efficiently overcomes the challenge of balancing variable formulation and process parameters. This method systematically investigates factor effects, yielding precise information with fewer experiments than studying factors individually [36]. The relationship between multiple variables and the corresponding responses was analyzed using response surface methodology (RSM). Statistical analysis, such as two-way Analysis of Variance (ANOVA), was employed to assess the significance of the generated parameters on the variables. A desirability function integrates responses into a single variable to predict optimal levels for independent variables. Desirability values span from 0 (representing an undesirable outcome) to 1 (reflecting the most favorable outcome) [37].

Using the QbD approach for nanosuspension formulation optimizes formulation and process parameters based on critical response parameters. The QbD approach for nanosuspension formation involves three steps: selecting suitable stabilizers and manufacturing processes, defining Critical Quality Attributes (CQAs), and establishing a Design Space. This study employed the QbD approach to develop stable Piribedil nanosuspensions using a sonication-assisted precipitation method. Following the optimization of the process, the subsequent step involved crafting nasal formulations by incorporating the pre-dispersions and sodium hyaluronate as a mucoadhesive agent.

MATERIALS AND METHODS

Materials

Piribedil was provided as a gift sample by Enomark Healthcare Pvt. Ltd., Dhamatwan, Gujarat, India. Poly (D, L-lactide-co-glycolide) was kindly supplied by DKC Hyderabad, India. The source of hyaluronic acid was Krishna Enterprises, New Delhi, India. Egg Yolk Lecithin Powder was procured from Gangwal Chemicals Pvt. Ltd., Mumbai, India. Analytical grade chemicals and solvents were exclusively employed for all supplementary experiments.

Methods

Nanosuspension preparation

The sonoprecipitation method was employed to create the nanosuspension of Piribedil, using a well-established procedure from previous studies [38]. Initially, Piribedil was completely dissolved in ethanol, resulting in a concentrated drug solution of approximately 10

mg/ml. The selected stabilizers were dissolved in triple distilled water. This solvent-antisolvent mixture was combined using a 22-gauge syringe and stirred continuously at 800 revolutions per minute (rpm) on a magnetic stirrer (REMI 1ML, Q-19) to induce drug precipitation. To further control particle growth under optimal conditions, the resulting suspension was subjected to sonication using a Probe sonicator (Vibra cell VCX 750 system, Sonics and Materials Inc.). During ultra-sonication, the ultrasound burst was set to 6 seconds on and 3 seconds off with 80% amplitude. After sonication, the nanosuspension was placed on a magnetic stirrer at 800 rpm for 3 h to ensure complete solvent evaporation. Subsequently, the prepared Piribedil nanosuspension was freeze-dried using a Lyodel Laboratory Scale Freeze Dryer (FD-01, Delvac Pumps Pvt. Ltd.) at a temperature of -54 °C under vacuum conditions. The final product was stored in an airtight container to ensure long-term preservation.

Optimization of formulation and process variables

Identification of critical quality attributes

Based on initial experimentation and existing scientific literature, critical quality attributes were identified, including particle size distribution, zeta potential, and practical yield [31]. The research underscored the significance of formulation variables like surfactant and polymer concentrations, as well as the solvent-to-antisolvent ratio. Additionally, the nanosuspension's characteristics were influenced by process variables like sonication time, amplitude, and infusion rate. Notably, these formulation and process variables were found to interact significantly. Given the complexity of optimizing multiple variables, the study adopted two separate designs of experiment approaches to streamline the optimization process for both formulation and process variables.

Experimental design for optimization of process parameters

The study identified three crucial factors, namely sonication time (A), sonication amplitude (B), and infusion rate (C), as having a significant influence on particle size (Y1), PDI (Y2), and zeta potential (Y3). Initial experiments were conducted to establish the suitable ranges for A, B, and C, as outlined in table 1. To comprehensively investigate how each independent formulation variable affects the response variables, we adopted a Box-Wilson Central Composite Design (CCD). This experimental design, encompassing three factors and five levels, was chosen for its suitability in evaluating quadratic response surfaces and developing second-order polynomial models for each corresponding response. The CCD incorporates a foundational factorial or fractional factorial design, supplemented by additional 'star points' to account for curvature [39]. The practical implementation of the experimental design and subsequent data analysis was facilitated using Stat-ease Design Expert® software V13.0.5.0. The designated experimental runs were conducted according to the design's specifications, with the obtained results inputted into the design for further analysis. The outcomes are detailed in table 2, and various statistical parameters were employed to analyze the responses.

Table 1: CCD-process variables and formulation with their levels

Process variables	Levels				
	- α	-1	0	+1	+ α
A-Sonication time	2.63	4	6	8	9.36
B-Sonication amplitude	33	50	75	100	117
C-Infusion rate	1.31	2	3	4	4.68
Response parameters	Objective				
Y1-Particle size	Minimize				
Y2-PDI	Minimize				
Y3-Zeta potential	Maximise				
Formulation variables	Levels				
	- α	-1	0	+1	+ α
A-Concentration of surfactant	0.33	0.5	0.75	1	1.17
B-Concentration of polymer	0.06	0.3	0.65	1	1.24
C-Solvent to antisolvent ratio	3.18	10	20	30	36.81
Response parameters	Objective				
R1-Particle size	Minimize				
R2-Zeta potential	Maximise				
R3-Practical yield	Maximise				

Table 2: The outcome of the experiments-optimization of process variables

Trial	Factors			Responses					
	A	B	C	Y1		Y2		Y3	
				Predicted	Actual	Predicted	Actual	Predicted	Actual
1	9.36	75	3	198.19	194.58	0.4666	0.457	-29.92	-29.56
2	4	50	4	514.45	514.78	0.7384	0.732	-21.14	-21.56
3	8	50	4	375.43	376.54	0.5159	0.526	-22.9	-22.87
4	6	75	3	106.29	103.56	0.3686	0.352	-29.65	-29.72
5	6	75	3	106.29	107.92	0.3686	0.364	-29.65	-30.19
6	6	75	3	106.29	101.56	0.3686	0.337	-29.65	-30.12
7	6	75	3	106.29	108.91	0.3686	0.398	-29.65	-28.76
8	8	100	4	83.49	86.38	0.3787	0.372	-27.73	-27.89
9	4	100	4	189.93	192.46	0.4503	0.446	-25.96	-26.12
10	8	50	2	247.92	249.54	0.4259	0.432	-28.82	-29.54
11	4	50	2	387.57	388.83	0.7045	0.713	-27.06	-26.78
12	4	100	2	269.78	272.82	0.4843	0.476	-28.44	-28.75
13	8	100	2	162.72	166.54	0.3568	0.365	-30.2	-30.27
14	6	75	3	106.29	111.12	0.3686	0.389	-29.65	-29.33
15	6	32.95	3	437.35	436.78	0.6380	0.628	-19.43	-19.12
16	6	75	4.68	260.4	258.32	0.4188	0.424	-26.12	-25.56
17	6	75	3	106.29	105.66	0.3686	0.372	-29.65	-30.52
18	6	117.04	3	92.83	87.53	0.3375	0.345	-24.65	-24.42
19	6	75	1.32	220.33	216.54	0.3718	0.364	-33.18	-32.56
20	2.64	75	3	405.13	402.87	0.7609	0.768	-26.96	-26.78

Experimental design for optimization of formulation parameters

Surfactant concentration (A), polymer concentration (B), and solvent-to-antisolvent ratio (C) were identified as crucial factors that impact particle size (R1), zeta potential (R2), and practical yield percentage (R3). The specified ranges for these critical variables were determined based on preliminary experiments, outlined in table 1. To thoroughly evaluate the influence of each independent formulation variable on the response variables, we opted for a Box-Wilson CCD characterized by three factors and five levels. The outcomes are detailed in table 3, and various statistical parameters were employed to analyze the responses.

Statistical treatment of obtained results

We utilized RSM to investigate how both formulation and process variables affected their respective response parameters. The outcomes derived from the trial experiments underwent statistical scrutiny via ANOVA. To visualize the influence of variables on response parameters, perturbation, response surface, and contour plots were employed. The quadratic influence of all variables on each response parameter was characterized using a polynomial prediction model [40]. The general polynomial equation, as depicted in Equation 1, serves as a representative illustration.

$$Y = \beta_0 + \beta_1 X_1 + \beta_2 X_2 + \beta_3 X_3 + \beta_{12} X_1 X_2 + \beta_{13} X_1 X_3 + \beta_{23} X_2 X_3 + \beta_{11} X_1^2 + \beta_{22} X_2^2 + \beta_{33} X_3^2 \dots \dots \dots (1)$$

Defining optimum levels of variables

The numerical optimization technique was employed to determine the optimal settings for each independent variable, ensuring the desired responses through the utilization of desirability values.

Verification of the optimum levels-Confirmation experiments

To validate the reliability of both designs, confirmation experiments were carried out using the determined optimal settings from each design. The prepared Piribedil nanosuspension was freeze-dried at a temperature of -54 °C under vacuum conditions. After preparation, the final product was carefully stored in an air-tight container to ensure its long-term preservation.

Characterization and evaluation of piribedil nanosuspension

Measurement of particle size distribution and zeta potential

The dynamic light scattering (DLS) technique was utilized to ascertain the particle size distribution of the nanosuspension. This technique provides valuable insights into the distribution of particle sizes in the sample. The nanosuspension was appropriately diluted

to ensure an optimal scattering intensity for accurate measurements. The key parameters, such as mean particle size and PDI were extracted from the analysis. Zeta potential, reflecting the electric potential on a particle's surface, serves as an indicator of colloidal system stability. The velocity of particle movement under the electric field (electrophoretic mobility) was measured. The measurement process was repeated multiple times to ensure accuracy and consistency.

Particle morphology

Inverse phase microscopy

This technique allows for visualizing and studying the nanosuspension samples. The Piribedil nanosuspension samples were appropriately prepared, ensuring they were well-dispersed. The nanosuspension samples were observed using the inverse phase microscopy technique. The preliminary characterization involved observing the dispersion of nanosized particles, potential aggregation, and the overall visual appearance of the nanosuspension.

Transmission Electron Microscopy (TEM)

TEM, a potent technique, facilitates the high-resolution imaging of nanoscale structures. The TEM instrument captures high-resolution images that offer intricate insights into the size, shape, and distribution of nanoparticles within the nanosuspension. A small drop of the Piribedil nanosuspension is placed onto a TEM grid and multiple images are captured from various areas of the grid to ensure representative sampling and to account for any heterogeneity in the sample. The captured TEM images are analyzed using appropriate software to measure particle sizes, observe their morphology, and assess their dispersion. Samples analyzed at 45000× intensification using transmission electron microscopy [30].

FTIR spectroscopy

FTIR spectroscopy is a method employed to identify and analyze specific chemical functional groups within a sample by detecting their distinctive absorption bands in the infrared region of the electromagnetic spectrum. FTIR spectra were recorded for Piribedil, Poly (lactic-co-glycolic acid; PLGA) 50:50, egg lecithin, and the Piribedil nanosuspension. The FTIR spectra obtained from the samples were analyzed to identify characteristic absorption bands associated with specific functional groups present in Piribedil and any other components in the nanosuspension.

Thermal analysis

Differential scanning calorimetry (DSC) was utilized for the thermal analysis of Piribedil, PLGA 50:50, egg lecithin, and the Piribedil

nanosuspension. The instrument was calibrated using standard reference materials. The sample, securely placed in a tightly closed standard aluminum pan, was subjected to a controlled temperature increase from ambient temperature (30 °C) to a predetermined upper-temperature limit (400 °C), at a uniform rate (10 °C/min). The observed heat flow changes were recorded to detect thermal transitions, such as melting points and crystallization, providing insights into the thermal behavior of the sample.

X-ray powder diffraction studies (XRD)

Powder XRD patterns of both plain Piribedil and Piribedil nanosuspension powder were captured and analyzed. The powder samples were subjected to scanning within a 2θ range of 10 to 60° at a scanning rate of 10°/min. As the X-rays interacted with the sample's crystalline structure, they underwent diffraction, producing a diffraction pattern. The resulting pattern provided information about the sample's crystallographic arrangement and the spacing of its lattice planes. The diffraction data were analyzed to identify the crystal phases present in the sample and to determine characteristics like crystal size and lattice parameters.

Saturation solubility of piribedil

Saturation solubility, defined as the maximum concentration of a drug that can dissolve in a given solvent under equilibrium, was determined by introducing an excess amount of Piribedil, its physical mixture, and nanosuspension into 5 ml of water or phosphate buffer solution (PBS) at pH 7.4 and 25 °C. After filtration, the drug concentrations in the filtrates were measured using a UV spectrophotometer at 239.2 nm.

Drug content estimation

Drug content analysis involved quantifying the quantity of drug within the formulated samples. For this purpose, a known quantity of the sample (10 mg) was dissolved in an appropriate solvent (50 ml of 0.1 N HCl). Following a 24 h stirring at room temperature using a magnetic stirrer set at 400 rpm, the solution was filtered and subjected to UV spectrophotometric analysis at a wavelength of 239.2 nm.

Drug release studies

Dissolution rates of Piribedil, the physical mixture, and the nanosuspension were assessed using the modified paddle method. Specifically, a quantity equivalent to 5 mg of pure Piribedil or nanosuspension was dissolved in 100 ml of PBS with a pH of 7.4. The experiment was carried out at 37 °C with the paddles rotating at 100 rpm. At predefined time intervals (5, 10, 15, 30, 60, 90, and 120 min), 5 ml aliquots were withdrawn and filtered. The concentration of Piribedil was determined using UV-Visible spectroscopy at a wavelength of 239.2 nm. To maintain sink conditions, withdrawn aliquots were replenished, and 0.1% Tween 80 was introduced into the dissolution medium.

Stability studies

To assess the stability of the nanosuspension, we took one milliliter of the formulation (equivalent to approximately 10 mg of Piribedil) and diluted it to various levels (10, 50, and 100 times) using milli-Q water. We then measured the particle size of each diluted sample using DLS. Next, we examined the nanosuspension's thermal stability under different storage temperatures (4, 25, and 35 °C) and monitored any morphological changes over the storage period. For the evaluation of storage stability, both the powdered and diluted nanosuspension were stored under different conditions (4 °C, 25 °C, and 40 °C/75% RH). At various time intervals, we analyzed critical parameters such as particle size and zeta potential to identify any alterations.

In situ gel preparation

The in-situ gel formulations were prepared by initially blending the required amount of lyophilized nanosuspension powder with the mucoadhesive agent hyaluronic acid. To achieve the desired concentrations, these formulations were suitably diluted with a 0.2% w/v solution of egg lecithin. Afterward, the prepared formulations were stored at 4 °C in a refrigerator for 24 h to ensure complete dissolution of the polymer. As a point of reference, we also

created parallel samples, referred to as reference samples. The final concentrations of Piribedil and hyaluronic acid in the nasal formulations and their corresponding reference samples are in the concentrations of 10 and 2 mg/ml, 10 and 5 mg/ml, and 10 and 10 mg/ml. Both the nasal formulations and reference samples contained equivalent amounts of Piribedil and hyaluronic acid, both dissolved in a 0.2% w/v egg lecithin solution. It's important to note that the Piribedil in the reference samples was added without undergoing any specific processing. In contrast, the reference samples were generated by using a ULTRA-TURRAX® homogenizer (GmbH, Germany) to homogenize raw Piribedil powder with hyaluronic acid and the 0.2% w/v egg lecithin solution. This homogenization process was conducted at 5000 rpm for 10 min.

In-situ gel formulation-characterization and evaluation

The pH of the intranasal formulations was determined by diluting them with distilled water and measuring the pH using a digital pH meter. For viscosity assessment, the intranasal formulations were analyzed using a Brookfield rotational viscometer (DV2T) fitted with a C 16-1 spindle, operating at a speed of 10 rpm.

To ascertain the drug content, a specific quantity of the formulation (10 mg) was dissolved in an appropriate solvent (50 ml of 0.1 N HCl). After stirring at room temperature with a magnetic stirrer at 400 rpm for 24 h, the solution was filtered and subsequently analyzed using a UV spectrophotometer at 239.2 nm.

The particle size of the intranasal formulations was determined using a particle size analyzer. To minimize light scattering effects, dilution with milli-Q water was carried out. Zeta potential measurements were conducted using the same instrument, with an additional electrode positioned on polystyrene electrophoretic cells. All measurements were performed in triplicate.

In vitro drug release study-in-situ gel formulation

The *in vitro* evaluation of drug release from the in-situ gel formulation was conducted using an artificial nasal fluid medium with specific concentrations of NaCl, KCl, and CaCl₂ while maintaining a pH of 5.6. The study commenced by placing 200 mg of both the intranasal formulation and its corresponding reference inside a dialysis bag. These bags were then inserted into a dialysis chamber and subjected to dialysis against 100 ml of the dissolution medium. The temperature was carefully maintained at 37±0.5 °C, while the paddle speed remained constant at 100 rpm. Throughout the experiment, 5 ml samples of the dissolution medium were collected at predetermined intervals. After each withdrawal, an equivalent volume of fresh dissolution medium was added to ensure consistent experimental conditions. For precise analysis, the collected samples were filtered through a 0.45µm filter before being assessed using a UV spectrophotometer set at 239.2 nm.

Permeability study (In vitro)

Permeability studies were conducted using a vertical Franz diffusion cell setup with synthetic polyvinylidene fluoride membranes tailored to the required dimensions. To enhance drug permeation, the membrane was pre-saturated with isopropyl myristate. In the donor phase, we placed 200 mg of the intranasal formulation on top of the membrane.

The vertical Franz diffusion cell system was carefully assembled. The membrane, loaded with the intranasal formulation, was positioned in the donor compartment. The acceptor compartment was filled with preheated PBS at pH 7.4 and maintained at 37 °C. Stirring was achieved using a magnetic stir bar in the acceptor compartment, set at 300 rpm. The diffusion study commenced and progressed at predetermined intervals. At each interval, 0.8 ml samples were extracted from the acceptor phase using an autosampler, and fresh phosphate buffer was added to maintain sink conditions.

The collected samples were then analyzed using a UV spectrophotometer at a wavelength of 239.2 nm to quantify the amount of Piribedil that had diffused. The drug's flux (J) was calculated by dividing the amount of Piribedil that permeated through the membrane by the surface area of the membrane insert

and the duration of the experiment, as shown in equation 2. Furthermore, the permeability coefficient (K_p) was determined using the obtained flux value (J) and the initial drug concentration in the donor phase, as described in Equation 3.

$$J = \frac{m}{A \cdot t} \dots (2)$$

where "m" represents the diffused quantity of Piribedil, "A" signifies the membrane insert's surface area, and "t" denotes the experiment's duration.

$$JK_p = \frac{J}{C_d} \dots \dots (3)$$

Where "C_d" stands for the initial concentration of the drug in the donor phase C

RESULTS AND DISCUSSION

The initial phase of the study involved a systematic exploration of various formulations and process conditions to identify suitable parameters for producing Piribedil nanosuspension. Particle size distribution, zeta potential values, and particle morphology were assessed to assess the developed formulations. Subsequently, egg lecithin and PLGA (50:50) were chosen as stabilizing agents for further investigation based on the outcomes of these preliminary experiments. From the outcomes of these preliminary experiments, the concentrations of egg lecithin (0.50-1.00 %w/v), PLGA-50:50 (0.3-1 % w/v), and the antisolvent to solvent ratio (10-30) were singled out for further optimization. Additionally, the influence of process parameters like sonication time, sonication amplification, and infusion rate on the final attributes of the Piribedil nanosuspension was recognized. Each parameter's optimum level was identified and refined through the use of a design of experiments approach.

Based on preliminary trial experiments, the determination of critical formulation and process parameters was undertaken. The investigation highlighted that essential quality attributes encompass particle size, PDI, zeta potential, and practical yield. Among the process parameters, sonication time, sonication amplification, and infusion rate were found to significantly impact the final

nanosuspension characteristics. Furthermore, the characteristics of the nanosuspension were found to be affected by formulation variables, including surfactant concentration, polymer concentration, and the ratio of antisolvent to solvent. To achieve optimal results and account for the interactive nature of process and formulation variables, a systematic statistical approach was preferred over the conventional one-factor-at-a-time (OFAT) approach. Hence, RSM was utilized to independently optimize both process and formulation variables. Through RSM, we examined how the independent variables were interrelated and forecasted the optimal conditions required to achieve the intended response. This methodology proves valuable by assessing interaction effects among chosen variables while minimizing the need for extensive experimental runs.

Process DoE-data analysis

A comprehensive set of twenty trials was undertaken, adhering to a CCD featuring three factors and five levels, to systematically optimize the process variables. Throughout these trials, the formulation variables, such as surfactant concentration (5% w/v), polymer concentration (0.5% w/v), and antisolvent to solvent ratio (20:1), were kept constant. The nanosuspension's average particle size (Y1) ranged from 86.38 to 514.78 nm, while the PDI (Y2) varied from 0.337 to 0.768. Furthermore, the zeta potential (Y3) exhibited a range between -32.56 and -19.12 mV.

The analysis of data and the establishment of regression equations were carried out, along with the calculation of ANOVA values and regression coefficients. A second-order quadratic model was employed to fit all experimental results. The model's adequacy was verified using ANOVA, lack of fit, and R-squared (R²) values. The superior fitting of the quadratic models was evident from the highest F values, as depicted in table 4. Multiple linear regression analysis was utilized to formulate mathematical equations for all the response variables. These derived equations proved to be statistically significant. The effectiveness of the model was assessed by examining the lack of fit values. Insignificant lack of fit values affirmed the model's efficiency. This was particularly notable since the lack of fit values for all models demonstrated insignificance, underscoring the model's aptness.

Table 4: ANOVA of the regression models-process DoE

Source	Sum of squares	df	Mean square	F-value	p-value	
Y1-particle size						
Model	3.42 x 10 ⁵	9	38005.07	2204.37	<0.0001	significant
A	51689.82	1	51689.82	2998.11	<0.0001	
B	1.43E+05	1	1.43E+05	8310.71	<0.0001	
C	1938.2	1	1938.2	112.42	<0.0001	
AB	530.89	1	530.89	30.79	0.0002	
BC	21369.68	1	21369.68	1239.48	<0.0001	
A ²	68760.88	1	68760.88	3988.26	<0.0001	
B ²	45428.63	1	45428.63	2634.95	<0.0001	
C ²	32383.75	1	32383.75	1878.32	<0.0001	
Residual	172.41	10	17.24			
Lack of Fit	109.5	5	21.9	1.74	0.2789	not significant
Pure Error	62.91	5	12.58			
Cor Total	3.42 x 10 ⁵	19				
Observed R ²	0.9995					
Adjusted R ²	0.9990					
CV	1.85					
Y2-PDI						
Model	0.3562	9	0.0396	115.55	<0.0001	significant
A	0.1046	1	0.1046	305.27	<0.0001	
B	0.109	1	0.109	318.13	<0.0001	
C	0.0027	1	0.0027	7.79	0.0191	
AB	0.0114	1	0.0114	33.28	0.0002	
BC	0.0023	1	0.0023	6.75	0.0266	
A ²	0.1083	1	0.1083	316.13	<0.0001	
B ²	0.0256	1	0.0256	74.7	<0.0001	
Residual	0.0034	10	0.0003			
Lack of Fit	0.0008	5	0.0002	0.3239	0.8792	not significant
Pure Error	0.0026	5	0.0005			

Source	Sum of squares	df	Mean square	F-value	p-value	
Cor Total	0.3596	19				
Observed R ²	0.9905					
Adjusted R ²	0.9819					
CV	4.00					
Y3-Zeta potential Model	215.99	9	24	66.33	<0.0001	significant
A	10.61	1	10.61	29.32	0.0003	
B	32.89	1	32.89	90.91	<0.0001	
C	60.2	1	60.2	166.39	<0.0001	
BC	5.92	1	5.92	16.35	0.0023	
A ²	2.8	1	2.8	7.74	0.0194	
B ²	105.33	1	105.33	291.12	<0.0001	
Residual	3.62	10	0.3618			
Lack of Fit	1.54	5	0.3081	0.7415	0.6246	not significant
Pure Error	2.08	5	0.4155			
Cor Total	219.61	19				
Observed R ²	0.9835					
Adjusted R ²	0.9687					
CV	2.19					

R² values, which indicate the variation around the mean, exceeded 0.98 for all response parameters, establishing the fitting of the model. However, relying solely on a higher R² value might not comprehensively determine model suitability, as additional variable terms could also contribute. Hence, considering the Adjusted R² value becomes essential. The regression coefficient (R²) values obtained for Y1, Y2, and Y3 were determined as 0.9995, 0.9904, and 0.9835, respectively. The consistency of both R² and adjusted R² values in both models signifies the elimination of non-significant terms.

Additionally, the coefficients of variation for the three responses were 1.85, 4.00, and 2.19, affirming the reproducibility and reliability of the models. Each experimental value is juxtaposed with the corresponding predicted value for all the response variables as indicated in table 2. These results unequivocally underscore the models' efficacy in identifying the essential process variables for the successful formulation of Piribedil nanosuspension.

Particle size (Y1)

Droplet size is crucial for nanosuspension evaluation. Smaller size increase medication absorption surface area. A smaller size may also speed release [21]. The nanosuspension's particle size spans between 86.38 and 514.78 nm. The particle diameter of the nanosuspension is notably influenced by the significant impact of factors A, B, and C, as indicated by the polynomial model. The polynomial equation for the particle size response demonstrates significance, evident from the substantial model F-value of 2724.82. The terms involving variables A, B, C, AB, BC, A², B², and C² were found to be statistically significant (P<0.05). The insignificant F-value of 1.45 for the lack of fit suggests a mere 34.93% probability of noise-induced high values. The non-significant lack of fit indicates the robustness of the model.

$$Y1 = 106.29 - 61.52A - 102.43B + 11.91C + 8.15AB - 51.68BC + 69.07A^2 + 56.15B^2 + 47.40C^2 \dots \dots (4)$$

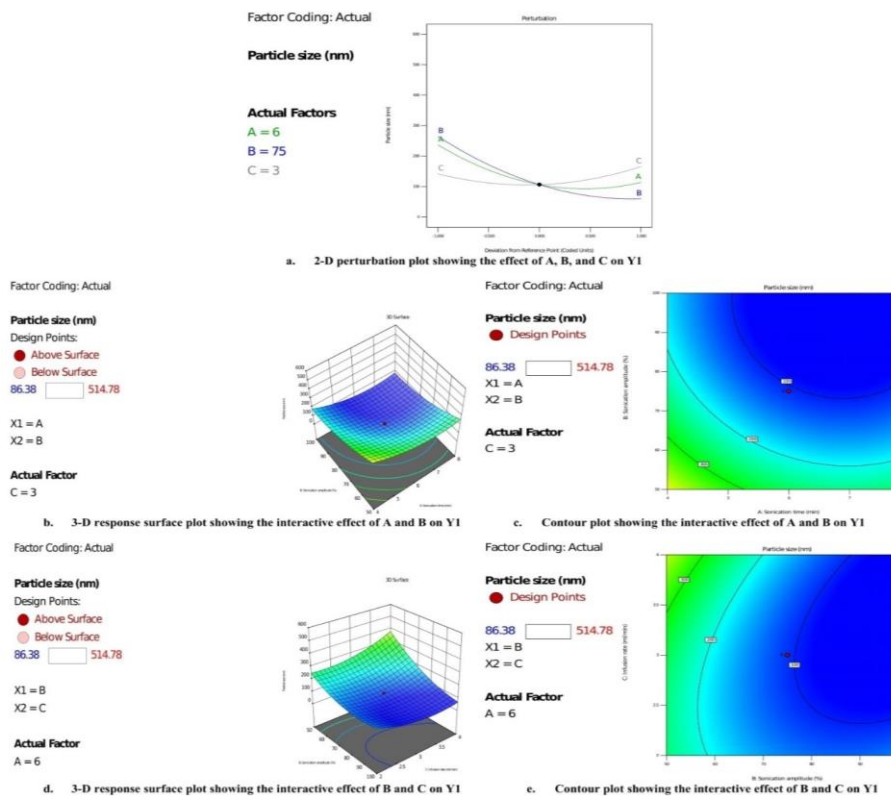


Fig. 1: 2-D perturbation plot, 3-D response surface plots, and contour plots showing effect on Y1

The equation underscores B's substantial influence on particle size. The model's R-squared (R²) value is 0.9995, and the adjusted R-squared value is 0.9991. The "Pred R-Squared" (0.9979) proximity to the "Adj R-Squared" value is notable. The "Adeq Precision" evaluates the signal-to-noise (S/N) ratio, where a value above 4 signifies a dependable model. Here, the model's S/N value of 162.298 supports its prediction reliability. This flexible model spans a broad design space.

For a clear grasp of variable effects on response (particle size), a two-dimensional perturbation plot was employed (fig. 1a). Independent variable B exerts a major influence, while variables A and C show intermediate effects. The interactive effects were illuminated by 3-D response surface and contour plots. Fig. 1b and 1c highlight significant interactions between factors A and B (AB) on Y1 (particle size), and the same is shown for factors B and C (BC) in fig. 1d and 1e.

Results show that augmenting sonication time and amplification reduces particle size. Conversely, higher infusion rates lead to larger particle sizes. With elevated sonication time, amplification, and infusion rate, particle size escalates exponentially. Positive interactive effects appear for A and B, while negative interaction is observed for B and C.

Poly dispersity index (PDI; Y2)

PDI gauges the uniformity of particle solutions, with larger values suggesting a wider size distribution within the sample. It also offers insights into particle aggregation, surface modifications' consistency, and sample analysis suitability [22]. Calculated through cumulants

analysis, this dimensionless index signifies the heterogeneity. A PDI below 0.05 signifies high uniformity, while values exceeding 0.7 imply an unsuitable sample for DLS. Ranging from 0.0 to 1.0, PDI numerically indicates distribution uniformity, with values below 0.2 (or 0.3 in lipid-based systems) generally accepted.

In the nanosuspension formulations, the PDI values varied between 0.3374 and 0.768, as indicated in table 2. The polynomial model highlighted factors A, B, and C's influence on percent drug loading. The correlation between practical and predicted values was good (table 2). The polynomial equation for PDI (Y2), represented by equation 5, showed significance with a model F-value of 115.55. Factors A, B, C, AB, BC, A², and B² displayed significance (p<0.05). The lack of fit's F-value (0.32) was insignificant, demonstrating an 87.92% probability of noise-induced high value, which is a favorable characteristic.

$$Y2 = 0.3686 - 0.0875A - 0.0893B + 0.0140C + 0.0378AB - 0.0170BC + 0.0867A^2 + 0.0421B^2 \dots \dots (5)$$

B and A stood out as more influential on PDI, evident from the equation. The model's R-squared (R²) and adjusted R² values were 0.9905 and 0.9819, respectively. The "Pred R-Squared" value (0.9712) aligns with "Adj R-Squared" (0.9819). The "Adeq Precision" value gauges the S/N ratio; an S/N above 4 signifies a reliable model. With an S/N of 32.3520, the model predicts well and adapts to broad design space. Two-dimensional perturbation plots (fig. 2a) reveal A and B's most significant impacts on PDI, while C has an intermediate influence. Three-dimensional response surfaces and contour plots (fig. 2b-2e) detail interactive effects among variables. These visuals provide insights into variable combinations and their PDI influence.

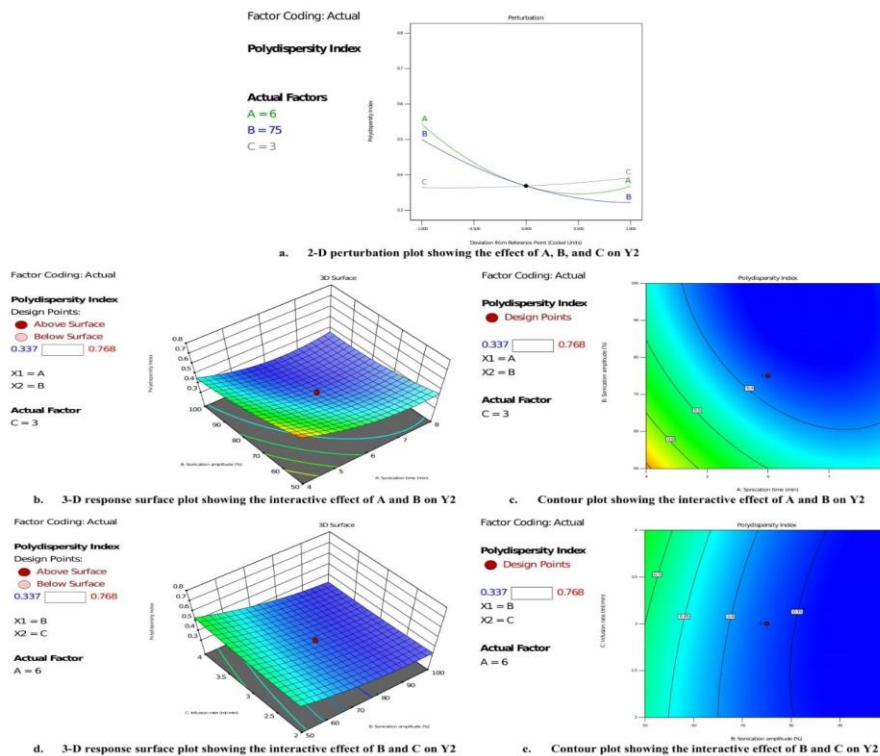


Fig. 2: 2-D perturbation plot, 3-D response surface plots, and contour plots showing effect on Y2

Zeta potential (Y3)

Zeta potential is a measure of nanosuspension stability at a macroscopic level. Electrostatically stabilized nanosuspensions usually require ±30 mV zeta potential, while ±20 mV is preferred for steric stabilization [22]. Zeta potential calculation involves determining electrophoretic mobility and converting it to zeta potential value. The zeta potential of the nanosuspension varied from -19.12 mV to -32.54 mV. The polynomial model indicated

variables A, B, and C's impact on nanosuspension yield, showing good practical-predicted correlation (table 2).

The polynomial equation (equation 6) for the zeta potential (Y3) was statistically significant, as indicated by a model F-value of 113.80. Factors A, B, C, BC, A², and B² also showed significance (P<0.05). An insignificant lack of fit F-value (0.61) suggests a 74.61% chance of noise-caused high value, favorable for a good model. C had more zeta potential influence (Y3) than other variables.

R² and adjusted R² values were 0.9813 and 0.9727. "Pred R-Squared" (0.9598) approximated "Adj R-Squared" (0.9727), reflecting good prediction. Adeq Precision (S/N ratio) at 41.3763 signifies model adequacy. The model's flexibility within a wide design space supports prediction.

$$Y3 = -29.75 - 0.8813A - 1.55B + 2.10C - 0.86BC + 0.4407A^2 + 2.70B^2 \dots \dots \dots (6)$$

Variable effects on zeta potential (Y3) were depicted in a two-dimensional perturbation plot (fig. 3a). C significantly affected zeta potential (Y3), while A and B had intermediate impacts. Interactive effects among variables were illustrated in 3-D response surfaces and contour plots. The substantial interaction between factors B and C (BC) and its impact on zeta potential (Y3) is illustrated in fig. 3b and 3c.

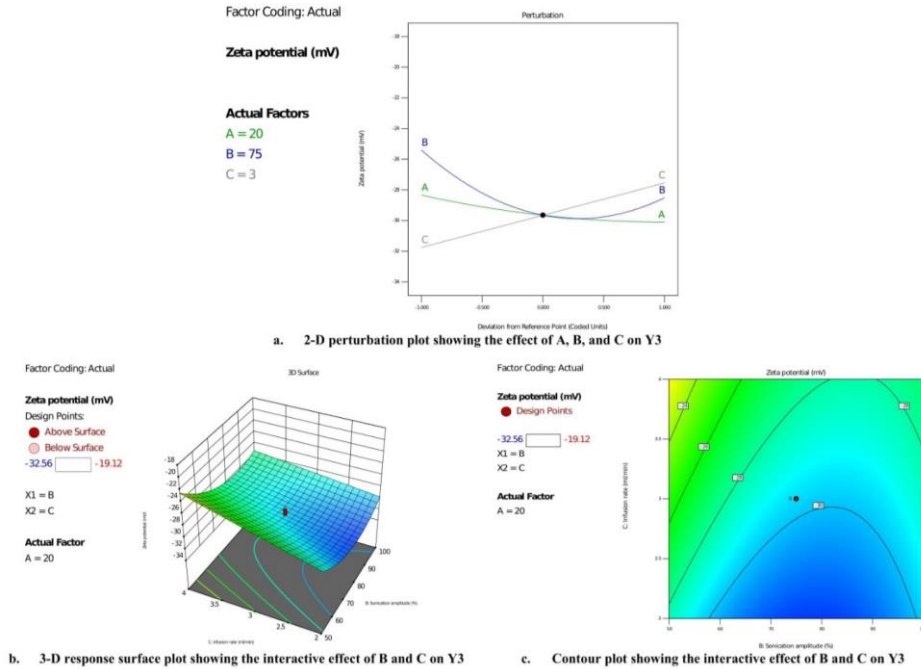


Fig. 3: 2-D perturbation plot, 3-D response surface plots, and contour plots showing effect on Y3

Optimization of process parameters

Numerical optimization was used to determine optimal levels for sonication time (A), sonication amplification (B), and infusion rate (C), impacting Y1, Y2, and Y3. Desirable constraints were applied to obtain optimum levels. The optimal process conditions were 7.08 min' sonication time, 83.44% sonication amplitude, and 2.4 ml/min infusion rate with a desirability value of 0.970.

Formulation DoE-data analysis

A comprehensive study involving twenty trials was executed using a 3-factor, 5-level CCD. During the formulation variable optimization, process variables were maintained at their optimal settings [24]. Recorded outcomes of these randomized experiments can be found in table 3. The prepared nanosuspension exhibited an average particle size (R1) ranging from 48.38 to 348.56 nm, zeta potential (R²) values between -34.56 to -30.93 mV, and practical yield (R3) spanning 64.78 to 98.34%.

Table 3: The outcome of the experiments-optimization of formulation variables

Trial	Factors			Responses					
	A	B	C	R1		R2		R3	
				Predicted	Actual	Predicted	Actual	Predicted	Actual
1	1.17	0.65	20	172.44	171.74	-34.35	-34.56	93.41	93.42
2	0.5	0.3	30	98.79	94.12	-28.24	-28.26	94.20	94.12
3	1	0.3	30	57.09	58.56	-34.22	-33.56	98.92	98.34
4	0.75	0.65	20	196.67	193.42	-31.80	-32.14	94.46	94.54
5	0.75	0.65	20	196.67	200.14	-31.80	-33.08	94.46	93.92
6	0.75	0.65	20	196.67	197.89	-31.80	-31.85	94.46	94.48
7	0.75	0.65	20	196.67	196.56	-31.80	-30.98	94.46	95.26
8	1	1	30	232.04	234.12	-34.15	-33.47	95.51	95.78
9	0.5	1	30	281.44	286.42	-25.51	-25.78	90.79	90.34
10	1	0.3	10	119.29	112.57	-34.22	-34.52	78.45	78.34
11	0.5	0.3	10	162.38	158.56	-28.24	-27.78	78.94	78.83
12	0.5	1	10	351.77	348.56	-25.51	-24.89	79.97	79.98
13	1	1	10	300.99	303.93	-34.15	-34.56	79.49	79.73
14	0.75	0.65	20	196.67	192.18	-31.80	-31.22	94.46	93.78
15	0.75	0.06	20	41.05	48.38	-32.98	-32.58	93.69	94.12
16	0.75	0.65	36.8	139.48	136.34	-31.80	-32.56	91.21	91.62
17	0.75	0.65	20	196.67	199.42	-31.80	-31.58	94.46	94.72
18	0.75	1.23	20	347.43	342.56	-30.62	-30.12	91.70	91.56
19	0.75	0.65	3.18	250.93	256.52	-31.80	-32.83	64.90	64.78
20	0.32	0.65	20	250.21	253.37	-22.06	-22.36	89.84	90.12

To assess relationships among independent variables and predict optimal conditions for desired responses, RSM was applied. RSM is effective in analyzing interaction effects while minimizing experimental runs. The results were subjected to analysis to derive ANOVA values,

regression coefficients, and equations. All the outcomes were fitted into a second-order quadratic model, and the model's adequacy was confirmed through ANOVA, lack of fit, and R^2 values. Table 5 presents models with the highest F values, indicating optimal fitting.

Table 5: ANOVA of the regression models-formulation DoE

Source	Sum of squares	Df	Mean square	F-value	p-value	
R1-Particle size						
Model	1.36E+05	9	15120.56	483.59	<0.0001	significant
A	7300.9	1	7300.9	233.5	<0.0001	
B	1.13E+05	1	1.13E+05	3623.92	<0.0001	
C	14994.11	1	14994.11	479.55	<0.0001	
A ²	386.86	1	386.86	12.37	0.0056	
Residual	312.67	10	31.27			
Lack of Fit	260.87	5	52.17	5.04	0.0503	not significant
Pure Error	51.8	5	10.36			
Cor Total	1.36E+05	19				
Observed R ²	0.9977					
Adjusted R ²	0.9956					
CV	2.81					
R2-Zeta potential						
Model	216.38	4	54.09	118.98	<0.0001	significant
A-Concentration of surfactant	182.46	1	182.46	401.32	<0.0001	
B-Concentration of polymer	6.69	1	6.69	14.71	0.0016	
AB	3.54	1	3.54	7.78	0.0137	
A ²	23.70	1	23.70	52.12	<0.0001	
Residual	6.82	15	0.4546			
Lack of Fit	4.01	10	0.4006	0.7120	0.6978	not significant
Pure Error	2.81	5	0.5627			
Cor Total	223.20	19				
Observed R ²	0.9694					
Adjusted R ²	0.9613					
CV	2.18					
R3-Practical yield						
Model	1366.63	8	170.83	714.54	<0.0001	significant
A-Concentration of surfactant	15.33	1	15.33	64.13	<0.0001	
B-Concentration of polymer	4.81	1	4.81	20.12	0.0009	
C-Ratio of two phases	835.82	1	835.82	3496.05	<0.0001	
AC	13.52	1	13.52	56.55	<0.0001	
BC	9.86	1	9.86	41.23	<0.0001	
A ²	14.45	1	14.45	60.45	<0.0001	
B ²	5.60	1	5.60	23.41	0.0005	
C ²	484.66	1	484.66	2027.22	<0.0001	
Residual	2.63	11	0.2391			
Lack of Fit	1.16	6	0.1937	0.6597	0.6886	not significant
Pure Error	1.47	5	0.2936			
Cor Total	1369.26	19				
Observed R ²	0.9981					
Adjusted R ²	0.9967					
CV	0.5470					

Mathematical equations were derived via multiple linear regression analysis for all response variables. The coefficients' magnitude corresponds to individual effects on response variables. Positive coefficients suggest synergistic effects, while negative values imply antagonistic effects. These equations exhibit statistical significance, and the lack of fit values for all models is insignificant, thus confirming the fitness of the models.

Multiple regression analysis results present R^2 , adjusted R^2 , and coefficient of variation values. R^2 values for all responses (R1, R2, and R3) were over 0.98, indicating model appropriateness. Adjusted R^2 is vital to evaluate model adequacy; the similarity between R^2 and adjusted R^2 values implies eliminated non-significant terms, enhancing model reliability. R^2 values for R1, R2, and R3 were 0.9977, 0.9694, and 0.9981, respectively, demonstrating the models' prediction accuracy. Coefficients of variation (2.81, 2.18, and 0.5470) confirm reproducibility and reliability.

Table 3 showcases a robust correlation between predicted and actual outcomes for all responses, validating the precise identification of process and formulation variables essential for

effective Piribedil nanosuspension formulation. This validation further underscores the models' reliability and effectiveness in optimizing nanosuspension formulation.

Particle size (R1)

Particle size determination holds paramount importance in assessing the efficacy of any nanoformulation. Size distribution plays a pivotal role in influencing stability, solubility, dissolution, and permeation across a variety of tissues and organs [36]. The nanosuspension's particle size ranges from 48.38 nm to 348.56 nm (table 3). The polynomial model underscores the substantial impact of factors A, B, and C on nanosuspension particle diameter. Observed values align closely with theoretical values, as detailed in table 3. The polynomial equation generated for the particle size response (equation 7) exhibits remarkable significance, demonstrated by its high model F-value of 483.59. Among the variable terms, A, B, C, and A² were found to be statistically significant ($p < 0.05$). The lack of fit F-value of 5.04, with only a 5.03% chance of noise interference, demonstrates the model's robustness. The significant influence of variable B on particle size is evident from the equation. The model's

regression coefficient (R^2) and adjusted R^2 values are 0.9977 and 0.9965, respectively. The close match between the "Pred R-Squared" value (0.9845) and the "Adj R-Squared" value (0.9956) further affirms the model's reliability. The Signal-to-noise (S/N) ratio, indicated by the "Adeq Precision" value of 78.585, reinforces its predictive accuracy. The two-dimensional perturbation plot (fig. 4a) succinctly illustrates the variables' impact on particle size. Variable B prominently affects particle size, while C and A exert intermediate effects. Interactive effects among variables are unveiled through three-dimensional response surface plots and corresponding

contour plots (fig. 4b and 4c). Importantly, the significant interactive effect between variables A and B (AB) on particle size (R1) is demonstrated. The results highlight how a polymer concentration increase leads to a larger particle size, while a higher concentration of surfactant leads to a smaller particle size. Furthermore, increasing the phase ratio results in reduced particle size. Noteworthy is the exponential particle size growth at elevated surfactant concentrations.

$$R1 = 196.67 - 23.12A + 91.09B - 33.13C + 5.18A^2 \dots \dots (7)$$

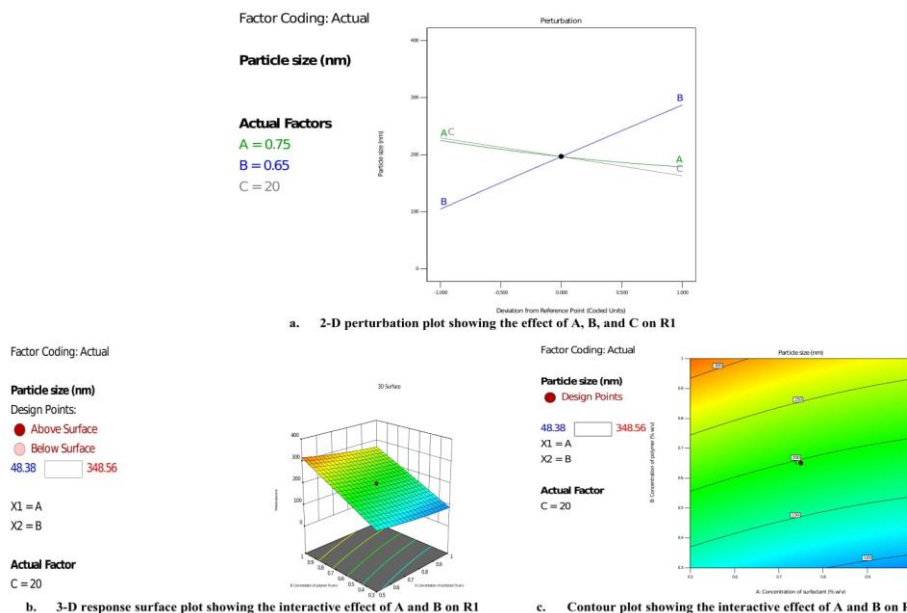


Fig. 4: 2-D perturbation plot, 3-D response surface plots, and contour plots showing effect on R1

Zeta potential (R2)

The zeta potential measurements for the nanoformulations exhibited a range between -34.56 and -30.93 mV. The zeta potential was significantly influenced by variables A and B according to the polynomial model. The practical and predicted values exhibited a strong correlation, as illustrated in table 3. The polynomial equation generated (equation 8) for the zeta potential response displayed significance, with a considerable model F-value of 118.98. Factors A, B, AB, and A^2 were determined to have significance ($p < 0.05$). The lack of fit F-value of 0.71 was not significant, suggesting a well-fitting model. Variable A exhibited a more significant influence on zeta potential value than other variables. The model's regression coefficient (R^2) and adjusted R^2 values were 0.9694 and 0.9613, respectively. The "Pred R-Squared" value of 0.9513 closely approximated the "Adj R-Squared" value of 0.9613. The "Adeq Precision" value, which measures the signal-to-noise (S/N) ratio, was 36.467, indicating a satisfactory model for prediction. The model was flexible and could be applied to a wide design space. The two-dimensional perturbation plot (fig. 5a) illustrated the individual effects of variables on zeta potential. Variable A had the most significant effect, while variables B and C had little effect. The interactive effects among the variables were visualized through the 3-D response surface and corresponding contour plots (fig. 5b and 5c). The significant interactive influence of variables A and B (AB) on zeta potential (R2) was observable. With increasing surfactant concentration, the zeta potential value increased from 93.56 to 85.12%.

$$R2 = -31.80 - 3.66A + 0.6998B - 0.6650AB + 1.27A^2 \dots \dots (8)$$

Percent practical yield (R3)

The practical yield of nanocrystals spanned from 64.78% to 98.34% (table 3). The polynomial model highlighted the substantial impact

of variables (A, B, and C) on nanocrystal practical yield. A favorable correlation was evident between practical and predicted values, as indicated in table 3. The formulated polynomial equation for the practical yield response yielded significance, boasting a robust model F-value of 714.54. The variable terms A, B, C, AC, BC, A^2 , B^2 , and C^2 displayed statistical significance ($p < 0.05$). The lack of fit F-value of 0.66, which was not significant, demonstrated a strong fit for the model. With only a 68.86% likelihood of noise-induced high values, this lack of fit insignificance highlighted the model's reliability. Importantly, variable C exhibited a more pronounced influence on practical yield compared to the other variables. The regression coefficient (R^2) and adjusted R^2 values for the model were 0.9981 and 0.9967, respectively. The "Pred R-Squared" value (0.9938) closely corresponded to the "Adj R-Squared" value (0.9967). The "Adeq Precision" value, gauging the signal-to-noise (S/N) ratio, tallied at 103.7252, indicating sound model prediction. The model's adaptability across an expansive design space was evident.

$$R3 = 94.46 + 1.06A - 0.5935B + 7.82C + 1.30AC - 1.11BC - 1.00A^2 - 0.6231B^2 - 5.80C^2 \dots \dots (9)$$

The two-dimensional perturbation plot (fig. 6a) depicted the individual effects of variables on practical yield. Variable C emerged as the most influential, while A and B exhibited intermediate and minor effects, respectively. The interactive effects among variables were unveiled through three-dimensional response surface and conforming contour plots (fig. 6b, 6c, 6d, and 6e). The significant interactive effects between A and C (AC) and B and C (BC) on practical yield (R3) were observed in these plots. The findings revealed that an escalation in polymer concentration correlated with a rise in practical yield, while an augmentation in surfactant concentration led to a reduction.

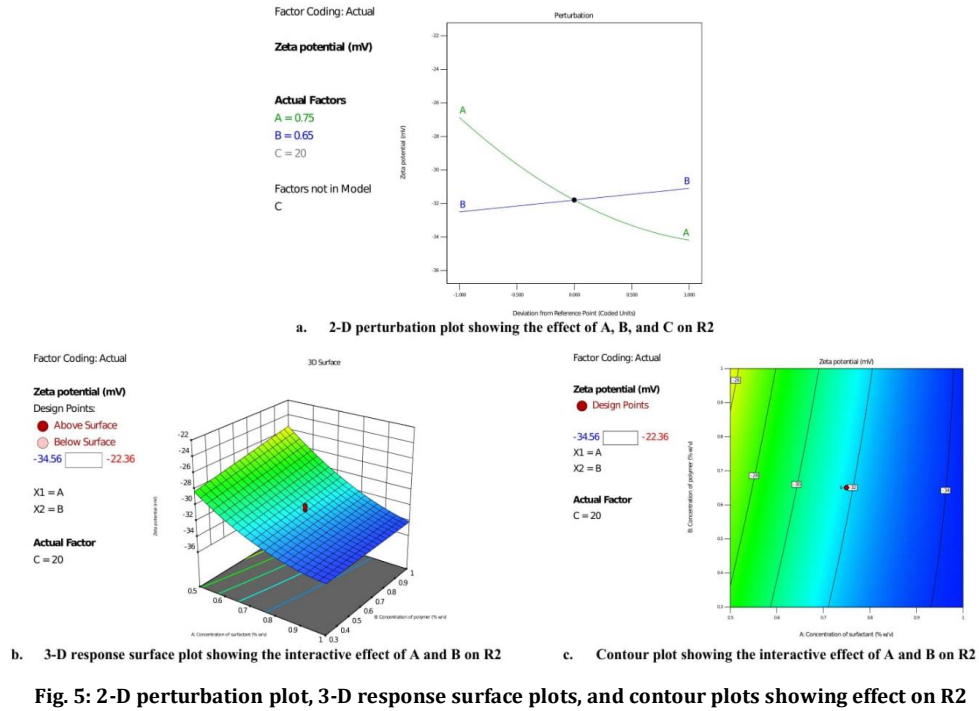


Fig. 5: 2-D perturbation plot, 3-D response surface plots, and contour plots showing effect on R2

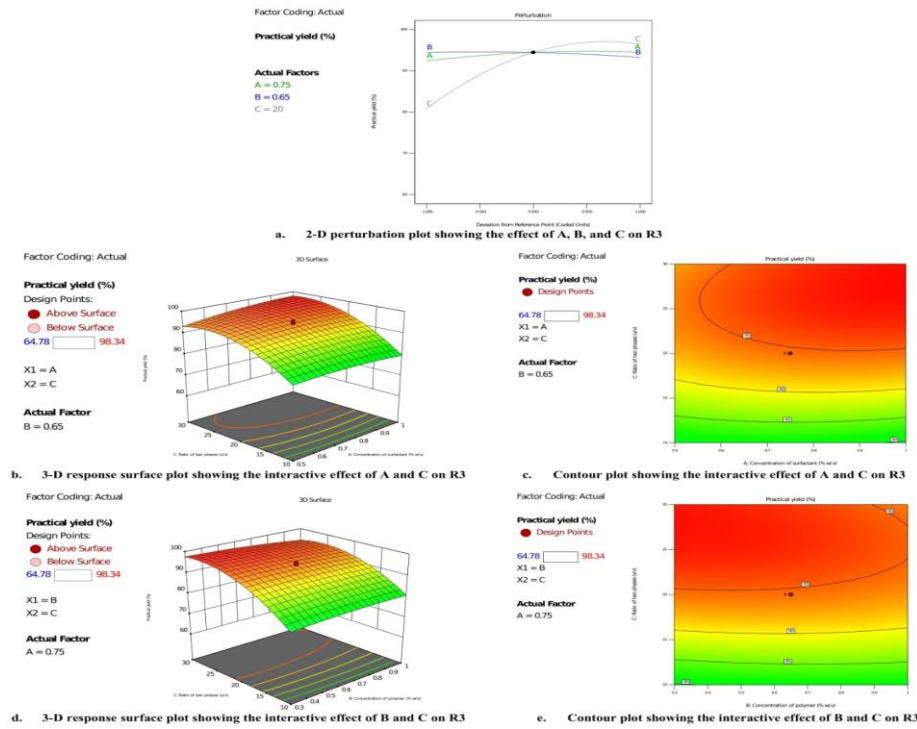


Fig. 6: 2-D perturbation plot, 3-D response surface plots, and Contour plots showing effect on R3

Optimal formulation parameter determination

Employing numerical optimization techniques with desirable constraints, the optimal levels of key process parameters were identified. These parameters, namely surfactant concentration (A), polymer concentration (B), and antisolvent to the solvent ratio (C), hold sway over particle size (R1), zeta potential (R2), and practical yield (R3). Specifically, the optimal conditions adopted for the method comprised a surfactant concentration of 1% w/v, a polymer concentration of 0.3% w/v, and an

antisolvent to solvent ratio of 30:1, with a desirability value of 0.981.

Formulation and process variable optimization

The investigation into optimizing the process and formulation variables, along with their effects on critical quality attributes, was facilitated using Derringer's desirability approach. The culmination of these optimal levels for critical formulation variables and process variables, alongside the anticipated values of response variables, are comprehensively outlined in table 6.

Table 6: The optimal values of Critical Process Parameters (CPPs) and Critical Formulation Parameters (CFPs), along with the predicted responses

Independent variables			
<i>Process (CPPs)</i>		<i>Formulation (CFPs)</i>	
Sonication time	7.09 min	Surfactant concentration	1 % w/v
Sonication amplification	83.44 %	Polymer concentration	0.3 % w/v
Infusion rate	2.41 ml/min	The ratio of the two phases	30:1
Desirability	0.970	Desirability	0.981
Critical quality attributes (predicted)			
Particle size (nm)	57.085		
PDI	0.3221		
Zeta potential (mV)	-34.229		
Practical yield (%)	98.9207		

Validation of the QbD approach

To assess the validation of the optimization process, three distinct batches ($n = 3$) of piribedil nanosuspension were produced utilizing the identified optimal levels of CPPs and CFPs. Subsequently, the experimental outcomes of the critical quality attributes were juxtaposed with the values forecasted by the model. The results obtained are in close agreement with the statistically projected values. The particle size values were between 46.7 ± 2.7 and 50.1 ± 3.4 nm. The PDI and zeta potential values were found to be as low as 0.393 ± 0.005 and -33.78 ± 1.86 mV and as high as 0.425 ± 0.005 and -35.06 ± 2.12 mV. Batch 1 showed highest practical yield i.e., $99.03 \pm 1.84\%$. This validation step reaffirms the accuracy and reliability of the QbD approach in achieving the desired outcomes for the nanosuspension formulation.

Characterization of as-prepared nanosuspension

The freshly prepared Piribedil nanosuspension exhibited an average particle size within the range of 46.7 nm to 50.1 nm, accompanied by PDI values spanning from 0.393 to 0.425. However, a slight increase in particle size was observed upon reconstitution of the freeze-dried nanosuspension, reaching 78.54 nm (with a PDI of 0.412). This size augmentation can be attributed to particle aggregation that occurred during the lyophilization process. The zeta potential values served

as indicators of the nanosuspension's stability. For the freeze-dried nanosuspension, zeta potential values were found to range from -33.78 ± 1.86 mV to -35.06 ± 2.12 mV, pointing toward favorable stability. Notably, a higher absolute zeta potential value (whether positive or negative) signifies improved dispersion and electrostatic repulsion among particles, contributing to enhanced stability.

The preliminary examination using inverse phase microscopy yielded valuable insights into the visual properties of the Piribedil nanosuspension, facilitating the initial evaluation of its dispersion and particle behavior. Microscopic images obtained through inverse phase microscopy revealed a particle size spectrum ranging from 50 nm to 80 nm. Upon lyophilization, the nanosuspension adopted an orange hue and appeared as irregular particles, as depicted in fig. 7a.

For a comprehensive understanding of the nanosuspension's nanoscale features and to validate the successful nanosuspension preparation process, TEM analysis was employed. This technique contributes complementary data to other characterization methods, aiding in the optimization of formulation parameters to achieve desired outcomes. The TEM image of the lyophilized nanosuspension is shown in fig. 7b, revealing the presence of smooth rod-like crystals. Notably, the particle size determined from both microscopic techniques closely aligned with the results obtained from the DLS method [34].

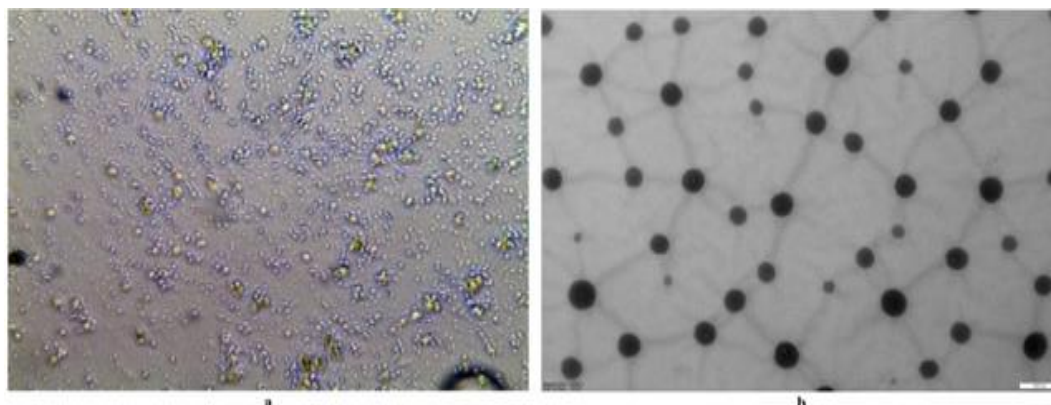


Fig. 7: (a). Microscopic image of Piribedil nanosuspension, (b). TEM image of Piribedil nanosuspension (Samples analyzed at 45000× intensification)

We used FTIR spectroscopy to see if Piribedil interacted with the stabilizers. In fig. 8a, you can see the FT-IR spectra of the different components and the nanoformulation. In the pure Piribedil spectra, we found strong signals at various wave numbers: 3025 cm^{-1} (related to aromatic C-H stretching), 2996 cm^{-1} (asymmetric and symmetric C-H stretching of CH_2), $2929\text{-}2858 \text{ cm}^{-1}$ (C-H stretching), $2825\text{-}2776 \text{ cm}^{-1}$ (C-H near oxygen), 1579 cm^{-1} (C-N stretching), 1546 cm^{-1} (conjugated C=C stretching), 1356 cm^{-1} (more conjugated C=C stretching), 1306 cm^{-1} (C-O stretching), 1251 cm^{-1} (asymmetric C-O stretching), 1112 cm^{-1} (C-N-C stretching), 1037 cm^{-1} (aromatic C-H stretching), and 976-

483 cm^{-1} (aliphatic C-H vibrations). In the FTIR spectrum of PLGA, we observed important peaks at 2924.18 cm^{-1} and 2852.81 cm^{-1} , which are related to C-H stretching. Additionally, there were bands at 1408.08 cm^{-1} , 1431.22 cm^{-1} , and 1467.87 cm^{-1} , associated with C=O bending vibrations. The FTIR spectrum of egg lecithin showed stretching bands at 2933.83 cm^{-1} and 2852.82 cm^{-1} , linked to the symmetric and asymmetric stretching of the -CH_2 group. Interestingly, in the FTIR spectra of the Piribedil nanosuspension, the distinctive peaks of Piribedil were no longer visible. These changes were likely due to Piribedil aggregating with PLGA.

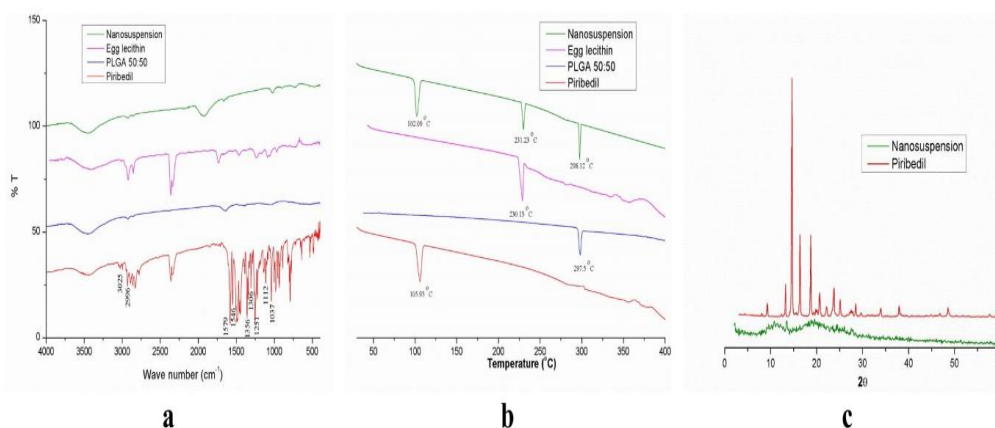


Fig. 8 (a): FTIR spectra of piribedil, PLGA, Egg lecithin, and nanosuspension; (b): DSC thermograms of Piribedil, PLGA, Egg lecithin, and nanosuspension; (c): XRPD pattern of Piribedil, and nanosuspension

DSC analysis was utilized to assess the aggregation state of Piribedil and PLGA within the nanosuspension. The DSC thermogram of free Piribedil displayed a sharp exothermic peak at 102.09 °C (fig. 8b), while the same peak was slightly altered and shifted (102.09 °C to 105.95 °C) in the case of the Piribedil nanosuspension. The observed shift in the characteristic peak could be attributed to a potential aggregation of Piribedil with the PLGA polymer [32]. Furthermore, the DSC thermogram of the nanosuspension indicated the presence of two distinct sharp endothermic peaks at 297.5 and 230.13 °C, suggesting the presence of both the polymer and surfactant in the formulation.

Pure Piribedil XRPD pattern displayed distinct crystalline 2θ peaks indicative of its crystalline nature. However, in the nanosuspension, the characteristic crystalline peaks vanished, giving rise to a halo and dim pattern typical of an amorphous substance (fig. 8c).

The solubility of Piribedil is recognized to be contingent on pH, displaying greater solubility at lower pH values. Notably, the nanosuspension exhibited increased solubility (1168.485±112.42µg/ml in water; 530.12±63.59µg/ml in PBS) compared to the pure drug (172.34±13.56 µg/ml in water; 122.34±15.34µg/ml in PBS). Specifically, the solubility of the nanoparticles increased by approximately 6.78-fold in water and 4.33-fold in pH 7.4 PBS (phosphate-buffered saline) compared to the pure drug. Sample quantities were chosen based on drug content analysis, which indicated measured drug content ranging from 96.3% to 98.4% compared to the theoretical drug content.

Fig. 9a provides a comprehensive view of the dissolution profiles of three different formulations: pure Piribedil, a physical mixture, and Piribedil nanosuspension. The tests were conducted using approximately 50 mg of the drug in PBS pH 7.4. The dissolution behavior of pure Piribedil showcased a relatively slow dissolution rate, with only 7.56% of the drug dissolving after 480 min. The physical mixture, on the other hand, exhibited a slightly improved dissolution rate of 19.912% after 120 min. This improvement is possibly a result of the enhanced wetting properties of the drug particles achieved through the mixture. In sharp contrast, the Piribedil nanosuspension exhibited a remarkable increase in dissolution performance compared to both the pure drug and the physical mixture. Around 18% of the drug was released from the nanosuspension within a mere 15 min, followed by a gradual release over the subsequent 8 h. This significant enhancement in drug release can be attributed to the decrease in particle size, which results in a larger surface area available for dissolution, following the principles of the Noyes-Whitney equation. Furthermore, the improved wetting properties of the drug particles likely contributed to the observed increase in the dissolution rate.

Stability assessment of piribedil nanosuspension

To ascertain the impact of storage conditions on the performance

attributes of the formulated nanocrystals, stability studies were meticulously conducted at temperatures of 4±2 °C, 25±2 °C, and 37±2 °C, spanning six months. Throughout this period, the mean particle size, PDI, and zeta potential values were monitored at regular intervals. These parameters were chosen as key indicators of the formulation's stability. The comprehensive results of these stability investigations provide compelling evidence that the Piribedil nanosuspension remains robust and stable over six months. This valuable information assures the formulation's shelf-life and reinforces its potential for practical applications.

Preparation and characterization of in-situ gel formulations

The in-situ gel formulations were meticulously crafted utilizing the lyophilized nanosuspension powder, augmented with the inclusion of hyaluronic acid. The formulation's final concentrations were finely controlled by dilution, employing 0.2% w/v of egg lecithin. The outcome was a series of intranasal formulations characterized by their discernible viscosity. The meticulous analysis of these formulations unveiled a consistent drug content exceeding 85%. Notably, the pH values of these samples harmoniously ranged from 6.0 to 6.4; adherence to the range suitable for nasal administration—a crucial consideration given the pH range of the nasal mucosa.

Upon assessment, it was evident that the addition of hyaluronic acid within the intranasal formulations exerted a transformative impact. Notably, the mean particle size, PDI, and zeta potential experienced a substantial elevation in the presence of hyaluronic acid. This increased particle size can be attributed to the coating of particles by hyaluronic acid. Furthermore, the incorporation of hyaluronic acid led to an augmentation in the negative charge within the formulation.

Dissolution of intranasal formulations

Due to Piribedil's inherent poor aqueous solubility, a pivotal consideration was to compare the dissolution profiles of the intranasal formulations with reference formulations containing pure Piribedil. Particularly noteworthy was the formulation designated as F2, which showcased the highest dissolution rate among the tested formulations. Impressively, F2 exhibited the release of approximately 56% of the drug within the initial 15 min. In contrast, the reference sample (R2) released only 8.56% of the drug within the same time frame. These substantial variations in dissolution rates can be attributed to the effects of nanosizing, where smaller particles generate a significantly larger surface area compared to their micro counterparts. Consequently, this enhanced surface area influences dissolution rates following the Noyes-Whitney equation [31]. Moreover, it's noteworthy that the nanosizing of Piribedil led to a notable 6.5-fold increase in saturation solubility compared to the raw drug. The dissolution profiles of these intranasal formulations, a vital indicator of their performance, are thoughtfully depicted in fig. 9b.

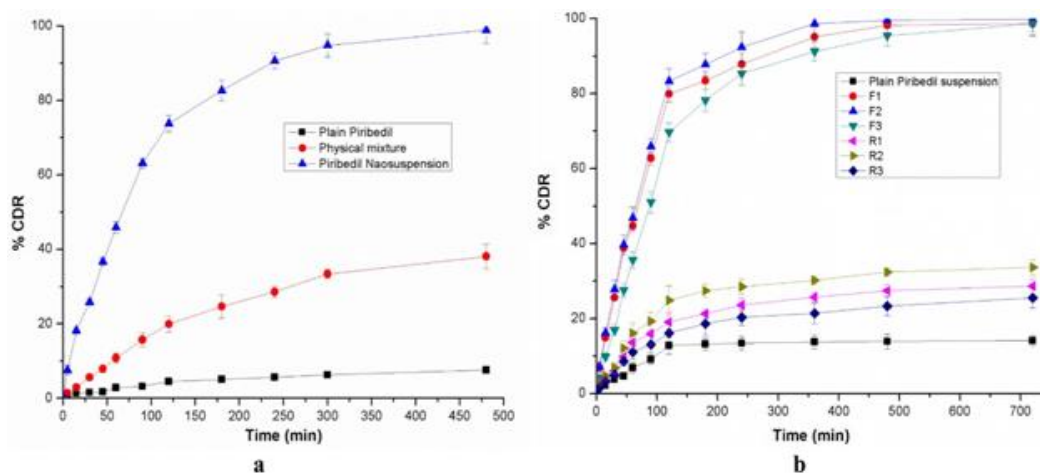


Fig. 9: (a). Dissolution pattern of piribedil nanosuspension, (b). Dissolution pattern of Piribedil intranasal formulations, Error bars indicate data in mean \pm SD, n=3

Permeation assessment and enhanced diffusion

The evaluation of diffusion serves as a critical indicator of permeation properties, elucidating the substance's ability to pass through barriers [35]. In the context of this study, the utilized membrane possessed a pore size of 100 nm, rendering the direct passage of Piribedil particles

unfeasible. Instead, the primary driving force behind passive diffusion rates was the substantial surface area achieved through the nanosizing of the particles. It's important to note that, owing to the larger surface area of the nanosized particles, diffusion from the intranasal formulations outpaced that of the reference samples, primarily due to heightened drug dissolution (as illustrated in fig. 10).

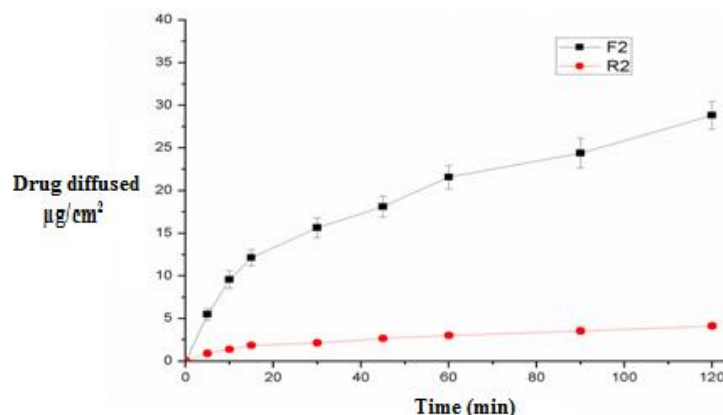


Fig. 10: *In vitro* permeability of intranasal formulations through a synthetic membrane using a Franz-diffusion cell at 37 °C, Error bars indicate data in mean \pm SD, n=3

Intriguingly, Piribedil exhibited immediate diffusion from the intranasal formulation (F2), in contrast to the reference formulation (R2) where diffusion commenced after 10 min. A notable disparity was observed in the flux (J), representing the amount of Piribedil traversing a 1 cm^2 membrane within 1 h. The formulation F2, incorporating Piribedil nanoparticles, demonstrated a significantly elevated J compared to the reference R2 (32.56 \pm 4.3 and 2.16 \pm 0.92 $\mu\text{g cm}^{-2} \text{ h}^{-1}$, respectively). This emphasized the facilitation of Piribedil penetration through the synthetic membrane by the hyaluronic acid-containing formulations. Remarkably, the flux of the nanosized-based formulation exceeded that of the reference containing pure Piribedil [38].

Additionally, the permeability coefficient (Kp) of F2 substantiated this trend by displaying a markedly higher value than R2, with Kp values measured at 0.094 and 0.013 cm. h^{-1} , respectively. Particularly noteworthy is the fact that within the initial 15 min, F2 saw the diffusion of 13.14 $\mu\text{g cm}^{-2}$ of the drug, compared to a mere 0.48 $\mu\text{g cm}^{-2}$ from R2. This elevated diffusion can be attributed to the amplified surface area achieved through nanoparticle formation, underscoring the advantageous impact of nanosizing on drug permeation [35]. As we delve deeper into the cutting-edge issue of

nanotechnology, it becomes clear that it is an important component of their use in a range of compositions to maximize the permeability of various medicinal substances. This ground-breaking combination of Piribedil nanosuspension with nasal administration has significant potential and is described in the literature as a game-changer. Notably, the created nanosystems are distinguished by their scalability and simplicity.

CONCLUSION

This study aimed to enhance the delivery of Piribedil to the brain via the nasal route through the development of an innovative approach. We successfully developed a nanosuspension incorporated into a nasal in-situ gelling system to improve the drug's transportation from the nasal cavity to the brain. This approach tackles the obstacles presented by the blood-brain barrier and holds promise for facilitating efficient drug delivery to the central nervous system. The nanosuspension formulation, characterized by small drug particles, serves to enhance drug solubility and bioavailability. Incorporating this nanosuspension into an in-situ gelling system further provides sustained drug release and prolonged drug residence time within the nasal cavity. Applying QbD principles, we

systematically optimized the formulation and process parameters of this innovative drug delivery system. By doing so, we aimed to enhance the efficiency and reliability of the delivery process. Our work pioneers the combination of nanosuspension and in-situ gelling for improved Piribedil delivery, opening up new possibilities for the administration of central nervous system drugs. This study not only illuminates a promising avenue for improving drug transport to the brain but also showcases the potential of employing QbD principles to optimize intricate drug delivery systems.

ACKNOWLEDGEMENT

The authors would like to thank the management of GITAM University in Hyderabad, Telangana, India, for providing the research facilities. They are also grateful to the department head and principal of Pharmaceutical Sciences at GITAM University in Hyderabad, Telangana, India, for their encouragement and assistance.

FUNDING

Nil

AUTHORS CONTRIBUTIONS

The contributions from each author are equal.

CONFLICT OF INTERESTS

The authors state that there are no real, potential, or perceived conflicts of interest in this research.

REFERENCES

- Achar A, Myers R, Ghosh C. Drug delivery challenges in brain disorders across the blood-brain barrier: novel methods and future considerations for improved therapy. *Biomedicines*. 2021 Dec;9(12):1834. doi: 10.3390/biomedicines9121834, PMID 34944650.
- Vidyadhari J, Gayatriramy M, Durga SPVN, Pavani P, Rajesh K. Nanosuspensions: a strategy to increase the solubility and bioavailability of poorly water-soluble drugs. *Asian J Pharm Clin Res*. 2023 May;16(5):33-40.
- Sowmya C, Suriyaprakash KK, Abrar AH. Solid lipid nanoparticles: modern progress in nose-to-brain transduction. *Int J Appl Pharm*. 2023 Apr;15(4):20-6.
- Partridge B, Eardley A, Morales BE, Campelo SN, Lorenzo MF, Mehta JN. Advancements in drug delivery methods for the treatment of brain disease. *Front Vet Sci*. 2022 Sep;9:1039745. doi: 10.3389/fvets.2022.1039745, PMID 36330152.
- Lee D, Minko T. Nanotherapeutics for Nose-to-brain drug delivery: an approach to bypass the blood-brain barrier. *Pharmaceutics*. 2021 Dec;13(12):2049. doi: 10.3390/pharmaceutics13122049, PMID 34959331.
- Bahadur S, Pardhi DM, Rautio J, Rosenholm JM, Pathak K. Intranasal nanoemulsions for direct nose-to-brain delivery of actives for CNS disorders. *Pharmaceutics*. 2020 Dec;12(12):1230. doi: 10.3390/pharmaceutics12121230, PMID 33352959.
- Khalifa NE, Nur AO, Osman ZA. Artemether loaded ethylcellulose nanosuspensions: effects of formulation variables, physical stability and drug release profile. *Int J Pharm Pharm Sci*. 2017 Jun;9(6):90-6. doi: 10.22159/ijpps.2017v9i6.18321.
- Grassin Delye S, Buenestado A, Naline E, Faisy C, Blouquit Laye S, Couderc LJ. Intranasal drug delivery: an efficient and non-invasive route for systemic administration: focus on opioids. *Pharmacol Ther*. 2012 Mar;134(3):366-79. doi: 10.1016/j.pharmthera.2012.03.003, PMID 22465159.
- Formica ML, Real DA, Picchio ML, Catlin E, Donnelly RF, Paredes AJ. On a highway to the brain: a review on nose-to-brain drug delivery using nanoparticles. *Appl Mater Today*. 2022 Jul;29:101631. doi: 10.1016/j.apmt.2022.101631.
- Saindane NS, Pagar KP, Vavia PR. Nanosuspension based in situ gelling nasal spray of carvedilol: development, *in vitro* and *in vivo* characterization. *AAPS PharmSciTech*. 2013 Jun;14(1):189-99. doi: 10.1208/s12249-012-9896-y, PMID 23255198.
- Hao J, Zhao J, Zhang S, Tong T, Zhuang Q, Jin K. Fabrication of an ionic-sensitive in situ gel loaded with resveratrol nanosuspensions intended for direct nose-to-brain delivery. *Colloids Surf B Biointerfaces*. 2016 Jan;147:376-86. doi: 10.1016/j.colsurfb.2016.08.011, PMID 27566226.
- Kürti L, Gaspar R, Marki A, Kapolna E, Bocsik A, Veszelka S. *In vitro* and *in vivo* characterization of meloxicam nanoparticles designed for nasal administration. *Eur J Pharm Sci*. 2013 Jan;50(1):86-92. doi: 10.1016/j.ejps.2013.03.012, PMID 23542493.
- Bartos C, Ambrus R, Sipos P, Budai Szucs M, Csanyi E, Gaspar R. Study of sodium hyaluronate-based intranasal formulations containing micro- or nanosized meloxicam particles. *Int J Pharm*. 2015 Jan;491(1-2):198-207. doi: 10.1016/j.ijpharm.2015.06.046, PMID 26142244.
- Mittur A. Piribedil: antiparkinsonian properties and potential clinical utility in dopaminergic disorders. *Curr Drug Ther*. 2011 Jan;6(1):17-34. doi: 10.2174/157488511794079004.
- Isaacson SH, Hauser RA, Pahwa R, Gray D, Duvvuri S. Dopamine agonists in Parkinson's disease: impact of D1-like or D2-like dopamine receptor subtype selectivity and avenues for future treatment. *Clin Park Relat Disord*. 2023 Jul;9:100212. doi: 10.1016/j.prdoa.2023.100212, PMID 37497384.
- Uppuluri CT, Ravi PR, Dalvi AV. Design, optimization and pharmacokinetic evaluation of piribedil-loaded solid lipid nanoparticles dispersed in nasal in situ gelling system for effective management of Parkinson's disease. *Int J Pharm*. 2021 Jun;606:120881. doi: 10.1016/j.ijpharm.2021.120881, PMID 34273426.
- Uppuluri CT, Ravi PR, Dalvi AV, Shaikh SS, Kale SR. Piribedil loaded thermo-responsive nasal in situ gelling system for enhanced delivery to the brain: formulation optimization, physical characterization, and *in vitro* and *in vivo* evaluation. *Drug Deliv Transl Res*. 2021 Nov;11(3):909-26. doi: 10.1007/s13346-020-00800-w, PMID 32514705.
- Tsai RS, El Tayar N, Carrupt PA, Testa B. Physicochemical properties and transport behaviour of piribedil: considerations on its membrane-crossing potential. *International Journal of Pharmaceutics*. 1992 Mar;80(1-3):39-49. doi: 10.1016/0378-5173(92)90260-9.
- Perez Lloret S, Rascol O. Piribedil for the treatment of motor and non-motor symptoms of parkinson disease. *CNS Drugs*. 2016 Jun;30(8):703-17. doi: 10.1007/s40263-016-0360-5, PMID 27344665.
- Yardımcı C, Suslu I, Ozaltın N. Determination of piribedil in pharmaceutical formulations by micellar electrokinetic capillary chromatography. *Anal Bioanal Chem*. 2004 Jul;379(2):308-11. doi: 10.1007/s00216-004-2539-8, PMID 14985904.
- Demirel M, Yazan Y, Muller RH, Kilic FA, Bozan B. Formulation and *in vitro-in vivo* evaluation of piribedil solid lipid micro and nanoparticles. *J Microencapsul*. 2001 Mar;18(3):359-71. doi: 10.1080/02652040010018119, PMID 11308226.
- Uppuluri CT, Ravi PR, Dalvi AV. Design and evaluation of thermo-responsive nasal in situ gelling system dispersed with piribedil-loaded lecithin-chitosan hybrid nanoparticles for improved brain availability. *Neuropharmacology*. 2021 Dec;201:108832. doi: 10.1016/j.neuropharm.2021.108832.
- Shete G, Bansal AK. NanoCrySP technology for generation of drug nanocrystals: translational aspects and business potential. *Drug Deliv Transl Res*. 2016 Aug;6(4):392-8. doi: 10.1007/s13346-016-0286-y, PMID 26912190.
- Junyaprasert VB, Morakul B. Nanocrystals for enhancement of oral bioavailability of poorly water-soluble drugs. *Asian J Pharm Sci*. 2015 Jan;10(1):13-23. doi: 10.1016/j.ajps.2014.08.005.
- Jacobs C, Kayser O, Muller RH. Production and characterisation of mucoadhesive nanosuspensions for the formulation of bupravaquone. *Int J Pharm*. 2001 Jan;214(1-2):3-7. doi: 10.1016/s0378-5173(00)00622-0, PMID 11282227.
- Aher SS, Malsane ST, Saudagar RB. Nanosuspension: an overview. *Int J Curr Pharm Sci* 2017;9(3):19-23. doi: 10.22159/ijcpr.2017.v9i3.19584.
- Patel VR, Agrawal YK. Nanosuspension: an approach to enhance solubility of drugs. *J Adv Pharm Technol Res*. 2011 Feb;2(2):81-7. doi: 10.4103/2231-4040.82950, PMID 22171298.
- Ranjita S. Nanosuspensions: a new approach for organ and cellular targeting in infectious diseases. *J Pharm Investg*. 2013 Jan;43(1):1-26. doi: 10.1007/s40005-013-0051-x.

29. Gigliobianco MR, Casadidio C, Censi R, Di Martino P. Nanocrystals of poorly soluble drugs: drug bioavailability and physicochemical stability. *Pharmaceutics*. 2018 Mar;10(3):134. doi: 10.3390/pharmaceutics10030134, PMID 30134537.
30. Ahire E, Thakkar S, Darshanwad M, Misra M. Parenteral nanosuspensions: a brief review from solubility enhancement to more novel and specific applications. *Acta Pharm Sin B*. 2018 May;8(5):733-55. doi: 10.1016/j.apsb.2018.07.011, PMID 30245962.
31. Ahmadi Tehrani A, Omranpoor MM, Vatanara A, Seyedabadi M, Ramezani V. Formation of nanosuspensions in a bottom-up approach: theories and optimization. *Daru*. 2019 Jun;27(1):451-73. doi: 10.1007/s40199-018-00235-2, PMID 30661188.
32. Peltonen L, Hirvonen J. Pharmaceutical nanocrystals by nanomilling: critical process parameters, particle fracturing and stabilization methods. *J Pharm Pharmacol*. 2010 Nov;62(11):1569-79. doi: 10.1111/j.2042-7158.2010.01022.x, PMID 21039542.
33. Pirincci Tok Y, Mesut B, Gungor S, Sarıkaya AO, Aldeniz EE, Dude U. Systematic screening study for the selection of proper stabilizers to produce physically stable canagliflozin nanosuspension by wet milling method. *Bioengineering (Basel)*. 2023 Aug;10(8):927. doi: 10.3390/bioengineering10080927, PMID 37627812.
34. Yu LX, Amidon G, Khan MA, Hoag SW, Polli J, Raju GK. Understanding pharmaceutical quality by design. *AAPS J*. 2014;16(4):771-83. doi: 10.1208/s12248-014-9598-3, PMID 24854893.
35. Simao J, Chaudhary SA, Ribeiro AJ. Implementation of quality by design (QbD) for development of bilayer tablets. *Eur J Pharm Sci*. 2023 May;184:106412. doi: 10.1016/j.ejps.2023.106412, PMID 36828037.
36. Mothilal M, Chaitanya KM, Surya Teja SP, Manimaran V, Damodharan N. Formulation and evaluation of naproxen-eudragit RS 100 nanosuspension using 3² factorial design. *Int J Pharm Pharm Sci*. 2014 Jul;6(7):449-55.
37. Pielenhofer J, Meiser SL, Gogoll K, Ciciliani AM, Denny M, Klak M. Quality by design (QbD) approach for a nanoparticulate imiquimod formulation as an investigational medicinal product. *Pharmaceutics*. 2023 Feb;15(2):514. doi: 10.3390/pharmaceutics15020514, PMID 36839835.
38. Pailla SR, Talluri S, Rangaraj N, Ramavath R, Challa VS, Doijad N. Intranasal zotepine nanosuspension: intended for improved brain distribution in rats. *Daru*. 2019 Dec;27(2):541-56. doi: 10.1007/s40199-019-00281-4, PMID 31256410.
39. Nagaraj K, Narendar D, Kishan V. Development of olmesartan medoxomil optimized nanosuspension using the box-behnken design to improve oral bioavailability. *Drug Dev Ind Pharm*. 2017 Jul;43(7):1186-96. doi: 10.1080/03639045.2017.1304955, PMID 28271908.
40. Rahman SNR, Katari O, Pawde DM, Boddeda GSB, Goswami A, Mutheneni SR. Application of design of experiments@ approach-driven artificial intelligence and machine learning for systematic optimization of reverse-phase high-performance liquid chromatography method to analyze simultaneously two drugs (cyclosporin a and etodolac) in solution, human plasma, nanocapsules, and emulsions. *AAPS PharmSciTech*. 2021 Apr;22(4):155. doi: 10.1208/s12249-021-02026-6, PMID 33987739.